

1 Potential transmission chains of variant

2 B.1.1.7 and co-mutations of SARS-CoV-2

3 Jingsong Zhang^{1#}, Yang Zhang^{2#}, Junyan Kang^{3,4}, Shuiye Chen², Yongqun He⁵, Benhao
4 Han¹, Mofang Liu^{3,4}, Lina Lu¹, Li Li⁶, Zhigang Yi^{2,7*} and Luonan Chen^{1,8,9,10*}

5

6 ¹State Key Laboratory of Cell Biology, Shanghai Institute of Biochemistry and Cell Biology,
7 Center for Excellence in Molecular Cell Science, Chinese Academy of Sciences, Shanghai
8 200031, China.

9 ²Key Laboratory of Medical Molecular Virology (MOE/NHC/CAMS), School of Basic Medical
10 Sciences, Shanghai Medical College, Fudan University, Shanghai 200032, China.

11 ³State Key Laboratory of Molecular Biology, Shanghai Key Laboratory of Molecular
12 Andrology, Shanghai Institute of Biochemistry and Cell Biology, Center for Excellence in
13 Molecular Cell Science, Chinese Academy of Sciences, Shanghai 200031, China.

14 ⁴University of Chinese Academy of Sciences, Shanghai 200031, China.

15 ⁵Department of Computational Medicine and Bioinformatics, University of Michigan Medical
16 School, Ann Arbor, MI 48109, USA.

17 ⁶Department of Genetics, Harvard Medical School, Boston, MA 02115, USA.

18 ⁷Shanghai Public Health Clinical Center, Fudan University, Shanghai 201508, China.

19 ⁸School of Life Science and Technology, ShanghaiTech University, Shanghai 201210, China.

20 ⁹ Key Laboratory of Systems Health Science of Zhejiang Province, Hangzhou Institute for
21 Advanced Study, University of Chinese Academy of Sciences, Hangzhou 310024, China.

22 ¹⁰ Pazhou Lab, Guangzhou 510330, China.

23 *Correspondence: Luonan Chen (lnchen@sibs.ac.cn) or Zhigang Yi (zgyi@fudan.edu.cn)

24 [#]These authors contributed equally: Jingsong Zhang, Yang Zhang

25 **Abstract**

26 The presence of SARS-CoV-2 mutants, including the emerging variant B.1.1.7, has raised
27 great concerns in terms of pathogenesis, transmission, and immune escape. Characterizing
28 SARS-CoV-2 mutations, evolution, and effects on infectivity and pathogenicity is crucial to
29 the design of antibody therapies and surveillance strategies. Here we analyzed 454,443
30 SARS-CoV-2 spike genes/proteins and 14,427 whole-genome sequences. We
31 demonstrated that the early variant B.1.1.7 may not have evolved spontaneously in the
32 United Kingdom or within human populations. Our extensive analyses suggested that
33 Canidae, Mustelidae or Felidae, especially the Canidae family (for example, dog) could be a
34 possible host of the direct progenitor of variant B.1.1.7. An alternative hypothesis is that the
35 variant was simply yet to be sampled. Notably, the SARS-CoV-2 whole genome represents a
36 large number of potential co-mutations with very strong statistical significances (p value<E–
37 44). In addition, we used an experimental SARS-CoV-2 reporter replicon system to introduce
38 the dominant co-mutations NSP12_c14408t, 5'UTR_c241t, and NSP3_c3037t into the viral
39 genome, and to monitor the effect of the mutations on viral replication. Our experimental
40 results demonstrated that the co-mutations significantly attenuated the viral replication. The
41 study provides valuable clues for discovering the transmission chains of variant B.1.1.7 and
42 understanding the evolutionary process of SARS-CoV-2.

43 **Key words:** SARS-CoV-2, variant B.1.1.7, transmission chains, co-mutations, viral
44 replication.

45 **Introduction**

46 Since the outbreak in December 2019, COVID-19 has been pandemic in over 200
47 countries. Cases of infection and mortalities have been surging and are an ongoing threat to
48 public health^{1,2}. COVID-19 is caused by infection with the novel coronavirus SARS-CoV-2³⁻⁵.
49 Although as a coronavirus, SARS-CoV-2 has genetic proofreading mechanisms⁶⁻⁸, the
50 persistent natural selection pressure in the population drives the virus to gradually
51 accumulate favorable mutations^{6,9,10}. Much attention has been paid to the mutations and
52 evolution of SARS-CoV-2¹¹⁻¹⁵, since mutations are related to the infectivity and pathogenicity
53 of viruses¹⁶⁻²¹. Beneficial mutants of the virus can better evolve and adapt to the host⁹, either
54 strengthening or weakening the infectivity and pathogenicity. In addition, certain variants
55 may generate drug resistance and reduce the efficacy of vaccines and therapeutics²²⁻²⁶. In
56 short, studying mutations and evolution in detail is vital to understand the transformations of
57 viral properties and to control the pandemic.

58 A new variant of SARS-CoV-2 named VOC-202012/01 (Variant of Concern 202012/01) or
59 lineage B.1.1.7 was first detected in the United Kingdom last December²⁷. It appears to be
60 substantially more transmissible than other variants²⁸. The variant has been growing
61 exponentially in the United Kingdom and rapidly spreading to other countries^{29,30}. However,
62 it is not yet clear if it evolved spontaneously in the United Kingdom or was imported from
63 other countries. Studying how the variant B.1.1.7 mutates can enable researchers to track its
64 spread over time and to understand the evolution of SARS-CoV-2.

65 In this study, large-scale SARS-CoV-2 sequences, consisting of more than 454,000 spike

66 genes/proteins and 14,000 whole-genome sequences were analyzed. Our extensive
67 sequence analysis showed that many mutations always co-occur not only in the spike
68 protein of B.1.1.7, but in the whole genome of SARS-CoV-2. The mutation trajectories of
69 the spike protein indicate that the early variant B.1.1.7 did not evolve spontaneously in the
70 United Kingdom or even within human populations. We also investigated possible
71 SARS-CoV-2 transmission chains of the variant B.1.1.7 based on the mutation analysis of
72 large-scale spike proteins and the cluster analysis of spike genes. Over the whole genome,
73 the top 25 high-frequency mutations of SARS-CoV-2 converged into several potential
74 co-mutation patterns, each of which showed a strong correlation with a very strong
75 statistical significance (p value<E-44). The potential co-mutations depicted the
76 evolutionary trajectory of SARS-CoV-2 virus in the population, shaping variable replication
77 of SARS-CoV-2. In addition, we further explored the effect of the dominant (co-)mutations
78 5'UTR_c241t, NSP3_c3037t, and NSP12_c14408t on viral replication using a
79 SARS-CoV-2 replicon based on a four plasmid *in-vitro* ligation system. The results
80 suggest that such mutations significantly attenuate the replication of SARS-CoV-2.

81 **Results**

82 **Evolutionary trajectories of variant B.1.1.7**

83 The variant B.1.1.7 was generally defined by multiple amino acid changes including 3
84 deletions (69-70del and 145del) and 7 mutations (N501Y, A570D, D614G, P681H, T716I,
85 S982A, and D1118H) in the spike protein³¹. The number of non-adjacent co-occurrent
86 changes indicates that they resulted from accumulated mutations. We therefore explored the

87 evolutionary trajectories of B.1.1.7 by tracing the incremental mutations ([Fig. 1a](#)). All routes
88 along the directions of the arrows are possible evolutionary trajectories of lineage B.1.1.7.
89 Among all the mutation routes, the green one was the most probable mutation trajectory
90 based on the number of variant strains. However, it was unlikely that the earliest variant
91 B.1.1.7 (GISaid: EPI_ISL_601443, 2020-09-20, England) with 9 mutations evolved from the
92 existing variants with 3–8 mutations, because the former arose much earlier than the latter.
93 More than 454,000 SARS-CoV-2 strains have been collected and extensively sequenced from
94 infected humans without finding intermediate variants with 3–9 mutations. It is therefore
95 unlikely that the intermediate variants with 3–8 mutations have infected humans. Thus, the
96 early variant B.1.1.7 might not have arisen spontaneously in the UK or within human
97 populations. An alternative hypothesis is that spillover likely occurred from susceptible
98 animals.

99 The co-appearance rates (see Materials and Methods) of all nine mutations are shown in
100 [Fig. 1b](#). We found that at least five mutations (145del, A570D, T716I, S982A, and D1118H)
101 of variant B.1.1.7 significantly co-occurred (rate>95%), which indicates a potential
102 co-mutation pattern in the spike protein, causing us to wonder what selection pressure drove
103 such co-occurrences of mutations and rapid evolution in the population of SARS-CoV-2.
104 Note that coronaviruses generally tend to exhibit rapid evolution when they jump to a
105 different species³². We therefore analyzed the key spike genes and proteins of existing
106 SARS-CoV-2 strains collected from animals to find a possible direct progenitor of variant
107 B.1.1.7. The variant with mutations “56” (labeled by “*” in [Fig. 1a](#), termed star variant) had
108 the minimum phylogenetic distance with EPI_ISL_699508, which was collected from a dog

109 on 2020-07-28 (Fig. 2) using MEGA^{33,34} (see Materials and Methods). The strains collected
110 from tigers, minks, and cats were also close to the star variant. Our extensive analyses
111 including mutations, phylogeny (Fig. 2), collection date/location and the number of
112 sequences (Tables S1-S3) suggested that Canidae, Mustelidae or Felidae, especially the
113 Canidae family (for example, dog) could be a possible host of the direct progenitor of variant
114 B.1.1.7. The possible transmission chains of variant B.1.1.7 are shown in Fig. 1c. This star
115 variant strains in humans could not have evolved into the early variant B.1.1.7, but they
116 might have infected high-density yet susceptible animals (such as dogs) and adapted to
117 these species through rapid mutation. Such progenitor variants comprised most or all of the
118 mutations of the early variant B.1.1.7 within the Canidae family populations, and they may
119 have spilled back to humans after the rapid mutation period.

120 **High-frequency mutations converge into potential co-mutations**

121 Based on sequence alignment and mutation analysis, we found that 7,441 nucleotide
122 alterations in the viral 29903-letter RNA code occurred at least once in the samples from
123 COVID-19 patients. These mutations were dispersed in the 14,427 SARS-CoV-2 strains
124 collected from all around the world. As shown in the heatmap of the top 1% high-frequency
125 mutations (Table S4), some sites show very similar mutation rates on most days in samples
126 isolated globally (Fig. S1), including 8,898 and 815 samples isolated from the U.S. (Fig. S2)
127 and Australia (Fig. S3). Therefore, these mutations shown in Fig. S4a were selected and
128 clustered into co-occurrences, which we called potential co-mutation patterns. From the
129 landscape of the mutation rates (Fig. S4a), 25 nucleotide sites were clearly clustered into

130 several potential co-mutation patterns. Among these patterns, there was one consisting of
131 the top 4 high-frequency mutations (i.e., 5'UTR_c241t, NSP3_c3037t, NSP12_c14408t, and
132 S_a23403g), which converged into a dominant potential co-mutation pattern. Such
133 co-occurrence lineage has been found in almost all sequenced samples of SARS-CoV-2.
134 Within this co-occurrence pattern, mutation S_a23403g resulted in the amino acid change
135 (D614G) that apparently enhances viral infectivity^{6,35}, albeit debate exists¹⁶. Notably, there
136 were three successive sites at the 28881st to 28883rd positions of the virus (N_g28881a,
137 N_g28882a, and N_g28883c) that strictly co-occurred. Comparing Fig. S4a-c and Table S4,
138 we found that the top 14 high-frequency mutations formed five common co-occurrence
139 patterns.

140 To assess the above co-occurrence patterns, we analyzed the correlations and statistical
141 significance levels of the high-frequency co-occurrence mutations. The heatmap of the
142 paired Pearson-correlation-coefficients (Fig. 3a) shows that the top 25 high-frequency
143 mutations clearly cluster into several potential co-mutation groups/patterns with very strong
144 correlation (≥ 0.8). By regression analyses, the above co-occurrence patterns have statistical
145 significance levels with p values less than 10^{-44} (Fig. 3b). The detailed mutation transitions
146 (Fig. 3c–k, Figs. S5–7) provide further evidence that the above mutations form co-mutation
147 patterns.

148 Dominant mutations attenuate viral replication

149 We further explored the effect of the dominant mutations 5'UTR_c241t, NSP3_c3037t,
150 and NSP12_c14408t on viral replication using a SARS-CoV-2 replicon based on a

151 four-plasmid *in-vitro* ligation system. This replicon is devoid of the viral structural proteins
152 while undergoing viral replication, and the viral replication is sensitive to the antiviral agent
153 remdesivir³⁶. The 5'UTR_c241t mutation resides in a highly conserved region in the 5'UTR
154 (Fig. 4a). The NSP3_c3037t mutation is synonymous. The NSP12_c14408t mutation is
155 nonsynonymous with an amino acid change of a conserved amino acid P323 in the viral
156 RNA-dependent RNA polymerase (Fig. 4b). We introduced the NSP12_c14408t mutation or
157 the NSP12_c14408t mutation with the other two mutations 5'UTR_c241t and NSP3_c3037t
158 into the replicon plasmids. The fragments were released from the plasmids by Bsal digestion,
159 and then assembled by *in-vitro* ligation with T4 ligase (Fig. 4c). Replicon RNA transcribed
160 from the ligation products was co-transfected with N mRNA into Huh7 cells. RNA replication
161 was monitored by measuring the secreted *Gaussia* luciferase activity in the supernatants.
162 Enzymatic dead mutants (759-SAA-761) of the RNA-dependent RNA polymerase NSP12
163 were introduced, and the mutated replicon served as a non-replication control. As shown in
164 Fig. 4d, transfection of WT replicon RNA resulted in an obvious increase of luciferase activity,
165 and SAA RNA did not replicate as expected. Introduction of NSP12_c14408t mutation
166 resulted in a significant reduction of viral replication. The combination of NSP12_c14408t
167 mutation with the other two mutations further significantly but only marginally reduced viral
168 replication. These results demonstrate that the P323L mutation in the viral RNA-dependent
169 RNA polymerase reduces viral replication, and the synonymous mutations may further
170 attenuate viral replication.

171 **Discussion**

172 A well-resolved phylogeny of variant B.1.1.7 spike genes provides an opportunity to
173 understand the evolutionary process and transmission chains of variant B.1.1.7. Our
174 incremental mutation and phylogenetic analyses on large-scale SARS-CoV-2 spike
175 proteins/genes revealed that the early variant B.1.1.7 might not have evolved spontaneously
176 in the United Kingdom or within human populations. In this case the spillover likely occurred
177 from susceptible animals. Current evidence³⁷⁻³⁹ indicates that SARS-CoV-2 can effectively
178 infect both domestic animals (for example, dog, cat, pig and bovine) and wild animals (for
179 example, mink, rabbit and fox) by binding their angiotensin converting enzyme 2 (ACE2).
180 Our further analyses including mutations, phylogeny, collection date/location and the
181 number of sequences suggested that the earliest variant B.1.1.7 possibly originated from
182 Canidae, Mustelidae or Felidae, especially the Canidae family (for example, dog). The
183 cases⁴⁰ that the variant B.1.1.7 can easily infect dogs and cats indicated that both are
184 susceptible to B.1.1.7. Still, due to the limited information available to date, an alternative
185 hypothesis is that the direct progenitor of variant B.1.1.7 is yet to be sampled. In addition to
186 variant B.1.1.7, as a future topic we will work on the analysis of other lineages such as P.1,
187 B.1.351, B.1.427, and B.1.42, when sufficient numbers of their sequences are available.

188 By tracing the mutation trajectories, we found that at least five mutations of the spike
189 proteins always co-occurred, and a large number of potential co-mutations appeared in the
190 top 1% high-frequency mutations of SARS-CoV-2 whole genome. It has been documented
191 that the mutation S_a23403g results in the amino acid change of the spike protein D614G

192 and enhances viral infectivity^{19,41-44}. Here, by using a SARS-CoV-2 reporter replicon system,
193 we demonstrated that the one of the dominant co-mutations NSP12_c14408t significantly
194 reduced viral replication and combination of NSP12_c14408t mutation with the other two
195 synonymous mutations 5'UTR_c241t and NSP3_c3037t although significantly but only
196 marginally reduced viral replication further. As the 5'UTR play an important role in regulating
197 viral replication, the synonymous mutations 5'UTR_c241t may attenuate viral replication by
198 change RNA secondary structure⁴⁵. These findings imply that SARS-CoV-2 undergoes an
199 evolution toward enhancing viral infectivity while attenuating viral replication. SARS-CoV-2
200 has exhibited significant mutations and co-mutations. We evaluated the replication of a
201 co-mutation pattern including three dominant mutations. If other mutations act similarly on
202 the viral replication needs to be verified. These results can be further explored for efficient
203 vaccine design in our future work. In summary, this study provides insights into the
204 transmission chains of variant B.1.1.7 and the effect of viral dominant mutations on viral
205 evolution.

206 **Materials and Methods**

207 **Data selection and pre-processing**

208 The 454,443 spike gene/protein sequences of SARS-CoV-2 were obtained at
209 <https://www.gisaid.org/>. The NCBI website at <https://www.ncbi.nlm.nih.gov/sars-cov-2/> has
210 released more than 1.7 thousand sequences of SARS-CoV-2 viruses before July 31, 2020.
211 We selected 14,427 sequences that satisfied two criteria: (1) having specific collection dates;
212 (2) sequence-lengths being no less than 29,305 nt (29903*0.98). It is inevitable that some

213 sites of sequences are equivocal owing to the limitation of sequencing depth. For instance,
214 many sites were labeled as letter N in genome sequences. The noise of indeterminate
215 nucleic-acids was taken into consideration in our experiments so as to boost accuracy. The
216 co-mutation rate of multi-site co-mutations was calculated by co – mutation rate =
217
$$\frac{\text{number of sequences containing co-mutations}}{\text{number of all sequences}}$$
. Moreover, the co-appearance rate of a mutation in
218 B.1.1.7 variant was defined by co – appearance rate =
$$\frac{\text{number of B.1.1.7 sequences}}{\text{number of sequences containing a mutation}}$$
.

219 **Possible animal host analyses**

220 In addition to the phylogenetic analysis, we further explored the possible animal hosts of
221 the direct progenitor of variant B.1.1.7 by mutations, collection time/space of strains, the
222 number of sequences and the edit distance^{46,47} of mutations (Table S1-2). Due to the late
223 lockdown policies of some governmental agencies, the spread of SARS-CoV-2 has not been
224 prevented well in Europe, America, and Australia. We could ignore the impact of policies for
225 studying the origin of variant B.1.1.7. We quantified the multiple impact factors of viral
226 transmission as shown in Table S3 based on the criterion that the smaller the value, the
227 more similar. The results still supported that the Canidae family is a possible host of the
228 direct progenitor of variant B.1.1.7.

229 **MEGA version and parameter settings**

230 Version: MEGA-X
231 Statistical Method: Maximum Likelihood
232 Test of Phylogeny: None
233 Model/Method: Jones-Taylor-Thornton (JTT) model

234 Rates among Sites: Uniform Rates
235 Gaps/Missing Data Treatment: Use all sites
236 ML Heuristic Method: Nearest-Neighbor-Interchange (NNT)
237 Initial Tree for ML: Make initial tree automatically (Default - NJ/BioNJ)
238 Branch Swap Filter: None
239 Number of Threads: 7

240 **Statistical analysis**

241 The Pearson-correlation-coefficient (PCC) is a classic statistic that measures linear
242 correlation between two variables. Its value ranges from -1.0 to 1.0. Normally, the two
243 variables meet a strong correlation or a very strong correlation when the absolute value of
244 PCC is between 0.6 and 0.8 or between 0.8 and 1.0. Linear regression is a linear approach
245 to model the relationship between a scalar response and one or more variables. We used
246 PCC and significance level (p value) of regression analysis to evaluate the relationships of
247 the co-occurrence mutations in large-scale SARS-CoV-2 examples.

248 **Plasmids**

249 Four plasmids encompassing the viral genome (pLC-nCoV-A-Bsal, pLC-nCoV-B-Bsal,
250 pLC-nCoV-C-Bsal, and pnCoV-D-sGluc-Bsal) were described previously³⁶. The
251 5'UTR_c-241-t and NSP3_c-3037-t mutations were introduced into the pLC-nCoV-A-Bsal by
252 fusion PCR. The NSP12_c-14408-t mutation was introduced into the pLC-nCoV-B-Bsal by
253 fusion PCR.

254 **Cell lines**

255 The human hepatoma cells Huh 7 were purchased from the Cell Bank of the Chinese
256 Academy of Sciences (www.cellbank.org.cn) and routinely maintained in Dulbecco's
257 modified medium supplemented with 10% FBS (Gibco) and 25 mM HEPES (Gibco).

258 ***In-vitro ligation***

259 Bsal digested fragments were gel purified using Gel Extraction Kit (OMEGA) and ligated
260 with T4 ligase (New England Biolabs) at room temperature for 1 h. The ligation products
261 were phenol/chloroform extracted, precipitated by absolute ethanol, and resuspended in
262 nuclease-free water, quantified by determining the A260 absorbance.

263 ***In-vitro transcription***

264 Purified *in-vitro* ligated product was used as template for the *in-vitro* transcription by
265 mMESSAGE mMACHINE T7 Transcription Kit (Ambion) according to the manufacturer's
266 protocol. For N mRNA production, we amplified the N coding region by PCR (sense: *GGC*
267 *ACA CCC CTT TGG CTC T*; antisense: *TTT TTT TTT TTT TTT TTT TTT TTT TTT TTT TTT*
268 *TTT TTT TCT AGG CCT GAG TTG AGT CAG CAC*) with phCMV-N as template. Then the
269 purified PCR product was used as a template for *in-vitro* transcription by mMESSAGE
270 mMACHINE T7 Transcription Kit as described above. RNA was purified by RNeasy mini
271 Elute (Qiagen), eluted in nuclease-free water, and quantified by UV absorbance (260 nm).

272 **Transfection**

273 Cells were seeded onto 48-well plates at a density of 7.5×10^4 per well and then

274 transfected with 0.3 μ g *in-vitro* transcribed RNA using a TransIT-mRNA transfection kit
275 (Mirus) according to the manufacturer's protocol.

276 **Luciferase activity**

277 Supernatants were taken from cell medium and mixed with equal volumes of 2 \times lysis
278 buffer (Promega). Luciferase activity was measured with Renilla luciferase substrate
279 (Promega) according to the manufacturer's protocol.

280 **Acknowledgments**

281 We thank associate prof. T.Z. and Dr. S.T.H. for useful comments on the manuscript. This
282 work is supported by the National Key Research and Development Program of China
283 (2017YFA0505500 to L.N.C., 2017YFC0909502 to J.S.Z.); the Strategic Priority Research
284 Program of the Chinese Academy of Sciences (XDB38040400 to L.N.C.); National Science
285 Foundation of China (31771476 and 31930022 to L.N.C, 61602460 and 11701379 to J.S.Z.);
286 Shanghai Municipal Science and Technology Major Project (2017SHZDZX01 to L.N.C.);
287 National Science and Technology Major Project of China (2017ZX10103009 to Z.G.Y.);
288 Emergency Project of Shanghai Science and Technology Committee (20411950103 to
289 Z.G.Y.); National Postdoctoral Program for Innovative Talent (BX20180331 to J.Y.K.); and
290 China Postdoctoral Science Foundation (2018M642018 to J.Y.K.).

291 **Author contributions**

292 L.N.C. and J.S.Z. designed the study. Z.G.Y. and J.S.Z. designed the experiments. J.S.Z.

293 analyzed data. Y. Z. performed the experiments of viral replication. J.S.Z., Z.G.Y., and J.Y.K.
294 designed the figures. S.C. repeated and checked the experiments of viral replication. H.B.H.
295 checked the computational analyses. J.S.Z. and Z.G.Y. wrote the manuscript. Y.Q.H, M.F.L.,
296 L.N.L, and L.L. polished the manuscript. All authors participated in result interpretation and
297 discussion.

298 **Data availability**

299 The raw sequence data reported in this paper have been deposited in the GISAID and NCBI
300 websites at <https://www.gisaid.org/> and <https://www.ncbi.nlm.nih.gov/sars-cov-2/>,
301 respectively. Code is available from the corresponding author on reasonable request.

302 **Conflict of interest**

303 The authors declare that they have no conflict of interest.

304 **References**

- 305 1 Wrapp, D. *et al.* Cryo-EM structure of the 2019-nCoV spike in the prefusion conformation. *Science* **367**,
306 1260-1263 (2020).
- 307 2 Chinazzi, M. *et al.* The effect of travel restrictions on the spread of the 2019 novel coronavirus (COVID-19)
308 outbreak. *Science*, 395-400 (2020).
- 309 3 Zhu, N. *et al.* A Novel Coronavirus from Patients with Pneumonia in China, 2019. *The New England journal of
310 medicine* **382**, 727-733, doi:10.1056/NEJMoa2001017 (2020).
- 311 4 Zhou, P. *et al.* A pneumonia outbreak associated with a new coronavirus of probable bat origin. *Nature* **579**,
312 270-273, doi:10.1038/s41586-020-2012-7 (2020).
- 313 5 Chen, L. *et al.* RNA based mNGS approach identifies a novel human coronavirus from two individual pneumonia
314 cases in 2019 Wuhan outbreak. *Emerging microbes & infections* **9**, 313-319,
315 doi:10.1080/22221751.2020.1725399 (2020).
- 316 6 Korber, B. *et al.* Tracking changes in SARS-CoV-2 Spike: evidence that D614G increases infectivity of the
317 COVID-19 virus. *Cell*, doi:doi.org/10.1016/j.cell.2020.06.043 (2020).
- 318 7 Smith, E. C., Blanc, H., Vignuzzi, M. & Denison, M. R. Coronaviruses Lacking Exoribonuclease Activity Are
319 Susceptible to Lethal Mutagenesis: Evidence for Proofreading and Potential Therapeutics. *Plos Pathog* **9** (2013).

320 8 Sevajol, M., Subissi, L., Decroly, E., Canard, B. & Imbert, I. Insights into RNA synthesis, capping, and
321 proofreading mechanisms of SARS-coronavirus. *Virus Res* **194**, 90-99 (2014).

322 9 Vignuzzi, M., Stone, J. K., Arnold, J. J., Cameron, C. E. & Andino, R. J. N. Quasispecies diversity determines
323 pathogenesis through cooperative interactions in a viral population. *439*, 344-348 (2006).

324 10 Garvin, M. R. *et al.* Potentially adaptive SARS-CoV-2 mutations discovered with novel spatiotemporal and
325 explainable AI models. *Genome Biology* **21**, 304, doi:10.1186/s13059-020-02191-0 (2020).

326 11 Tang, X. *et al.* On the origin and continuing evolution of SARS-CoV-2. *National Science Review* **7**, 1012-1023,
327 doi:10.1093/nsr/nwaa036 %J National Science Review (2020).

328 12 Acter, T. *et al.* Evolution of severe acute respiratory syndrome coronavirus 2 (SARS-CoV-2) as coronavirus
329 disease 2019 (COVID-19) pandemic: A global health emergency. *Science of The Total Environment* **730**, 138996,
330 doi:<https://doi.org/10.1016/j.scitotenv.2020.138996> (2020).

331 13 Plante, J. A. *et al.* Spike mutation D614G alters SARS-CoV-2 fitness. *Nature*, doi:10.1038/s41586-020-2895-3
332 (2020).

333 14 Zohar, T. *et al.* Compromised Humoral Functional Evolution Tracks with SARS-CoV-2 Mortality. *Cell* **183**,
334 1508-1519.e1512, doi:10.1016/j.cell.2020.10.052 (2020).

335 15 Li, T. *et al.* The use of SARS-CoV-2-related coronaviruses from bats and pangolins to polarize mutations in
336 SARS-CoV-2. *Science China Life Sciences* **63**, 1608-1611, doi:10.1007/s11427-020-1764-2 (2020).

337 16 Grubaugh, N. D., Hanage, W. P. & Rasmussen, A. L. Making sense of mutation: what D614G means for the
338 COVID-19 pandemic remains unclear. *Cell*, doi:doi.org/10.1016/j.cell.2020.06.040 (2020).

339 17 Liu, Z. *et al.* Identification of Common Deletions in the Spike Protein of Severe Acute Respiratory Syndrome
340 Coronavirus 2. *J Virol* **94** (2020).

341 18 Li, Q. Q. *et al.* The Impact of Mutations in SARS-CoV-2 Spike on Viral Infectivity and Antigenicity. *Cell* **182**,
342 1284-+ (2020).

343 19 Plante, J. A. *et al.* Spike mutation D614G alters SARS-CoV-2 fitness. *Nature* (2020).

344 20 Blanco, J. D., Hernandez-Alias, X., Cianferoni, D. & Serrano, L. In silico mutagenesis of human ACE2 with S
345 protein and translational efficiency explain SARS-CoV-2 infectivity in different species. *Plos Comput Biol* **16**
346 (2020).

347 21 Zhang, L. Z. *et al.* SARS-CoV-2 spike-protein D614G mutation increases virion spike density and infectivity. *Nat
348 Commun* **11** (2020).

349 22 A., B. *et al.* Antibody cocktail to SARS-CoV-2 spike protein prevents rapid mutational escape seen with
350 individual antibodies. *Science*, doi:10.1126/science.abd0831 (2020).

351 23 Hansen, J. *et al.* Studies in humanized mice and convalescent humans yield a SARS-CoV-2 antibody cocktail.
352 *Science*, doi:10.1126/science.abd0827 (2020).

353 24 Sheahan, T. P. *et al.* An orally bioavailable broad-spectrum antiviral inhibits SARS-CoV-2 in human airway
354 epithelial cell cultures and multiple coronaviruses in mice. *Sci Transl Med* **12** (2020).

355 25 Nunes-Santos, C. J., Kuehn, H. S. & Rosenzweig, S. D. N-Glycan Modification in Covid-19 Pathophysiology: In
356 vitro Structural Changes with Limited Functional Effects. *J Clin Immunol* (2020).

357 26 Lo, M. K. *et al.* Remdesivir targets a structurally analogous region of the Ebola virus and SARS-CoV-2
358 polymerases. *P Natl Acad Sci USA* **117**, 26946-26954 (2020).

359 27 Editorial. Evolution goes viral. *Nature Ecology & Evolution* **5**, 143-143, doi:10.1038/s41559-021-01395-2 (2021).

360 28 Editorial. COVID-19 vaccines: acting on the evidence. *Nature Medicine*, doi:10.1038/s41591-021-01261-5
361 (2021).

362 29 Muik, A. *et al.* Neutralization of SARS-CoV-2 lineage B.1.1.7 pseudovirus by BNT162b2 vaccine-elicited human
363 sera. eabg6105, doi:10.1126/science.abg6105 %J Science (2021).

364 30 Rice, B. L. *et al.* Variation in SARS-CoV-2 outbreaks across sub-Saharan Africa. *Nature Medicine*,
365 doi:10.1038/s41591-021-01234-8 (2021).

366 31 Muik, A. *et al.* Neutralization of SARS-CoV-2 lineage B.1.1.7 pseudovirus by BNT162b2 vaccine–elicited human
367 sera. *Science*, eabg6105, doi:10.1126/science.abg6105 %J Science (2021).

368 32 Zhou, P. & Shi, Z.-L. SARS-CoV-2 spillover events. *Science* **371**, 120-122, doi:10.1126/science.abf6097 %J Science
369 (2021).

370 33 Kumar, S., Stecher, G., Li, M., Knyaz, C. & Tamura, K. MEGA X: Molecular Evolutionary Genetics Analysis across
371 Computing Platforms. *Molecular Biology and Evolution* **35**, 1547-1549 (2018).

372 34 Tamura, K. & Nei, M. Estimation of the Number of Nucleotide Substitutions in the Control Region of
373 Mitochondrial-DNA in Humans and Chimpanzees. *Molecular Biology and Evolution* **10**, 512-526 (1993).

374 35 Li, Q. *et al.* The impact of mutations in SARS-CoV-2 spike on viral infectivity and antigenicity. *Cell*,
375 doi:doi.org/10.1016/j.cell.2020.07.012 (2020).

376 36 Zhang, Y., Song, W., Chen, S., Yuan, Z. & Yi, Z. A bacterial artificial chromosome (BAC)-vectored noninfectious
377 replicon of SARS-CoV-2. *bioRxiv*, doi:doi.org/10.1101/2020.09.11.294330 (2020).

378 37 Shi, J. *et al.* Susceptibility of ferrets, cats, dogs, and other domesticated animals to SARS–coronavirus 2. *Science*
379 **368**, 1016-1020, doi:10.1126/science.abb7015 %J Science (2020).

380 38 Wu, L. *et al.* Broad host range of SARS-CoV-2 and the molecular basis for SARS-CoV-2 binding to cat ACE2. *Cell*
381 Discovery **6**, 68, doi:10.1038/s41421-020-00210-9 (2020).

382 39 Patterson, E. I. *et al.* Evidence of exposure to SARS-CoV-2 in cats and dogs from households in Italy. *Nat*
383 *Commun* **11**, 6231, doi:10.1038/s41467-020-20097-0 (2020).

384 40 Ferasin, L. *et al.* Myocarditis in naturally infected pets with the British variant of COVID-19. *bioRxiv*,
385 2021.2003.2018.435945, doi:10.1101/2021.03.18.435945 %J bioRxiv (2021).

386 41 Raghav, S. *et al.* Analysis of Indian SARS-CoV-2 Genomes Reveals Prevalence of D614G Mutation in Spike
387 Protein Predicting an Increase in Interaction With TMPRSS2 and Virus Infectivity. *Front Microbiol* **11** (2020).

388 42 Johnson, M. C. *et al.* Optimized Pseudotyping Conditions for the SARS-CoV-2 Spike Glycoprotein. *J Virol* **94**
389 (2020).

390 43 Jiang, X. Y. *et al.* Bimodular effects of D614G mutation on the spike glycoprotein of SARS-CoV-2 enhance
391 protein processing, membrane fusion, and viral infectivity. *Signal Transduct Tar* **5** (2020).

392 44 Fernandez, A. Structural Impact of Mutation D614G in SARS-CoV-2 Spike Protein: Enhanced Infectivity and
393 Therapeutic Opportunity. *AcS Medicinal Chemistry Letters* **11**, 1667-1670 (2020).

394 45 Sun, L. *et al.* *In vivo* structural characterization of the SARS-CoV-2 RNA genome identifies
395 host proteins vulnerable to repurposed drugs. *Cell* **184**, 1865-1883.e1820, doi:10.1016/j.cell.2021.02.008
396 (2021).

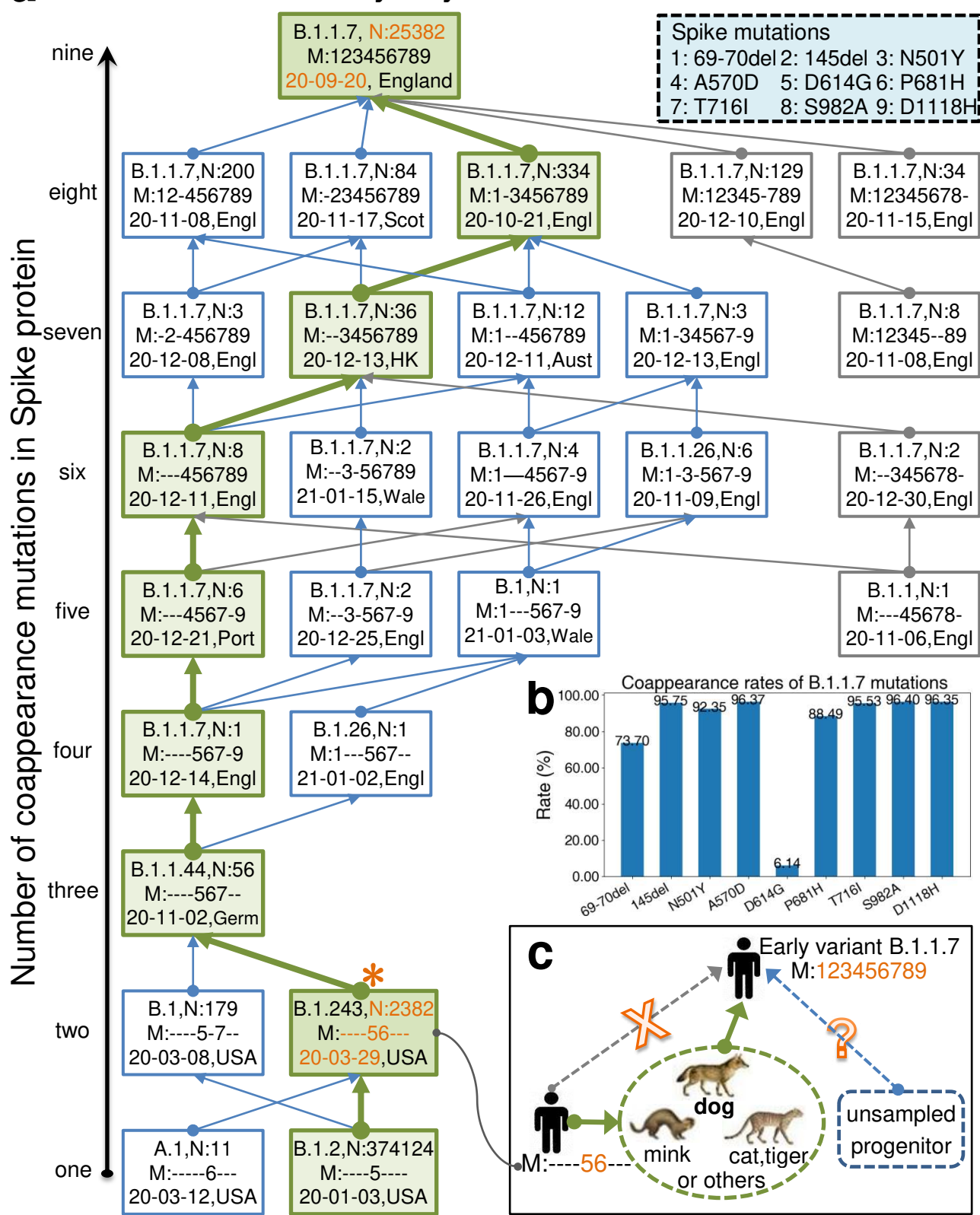
397 46 Ristad, E. S., Yianilos, P. N. J. I. T. o. P. A. & Intelligence, M. Learning string-edit distance. *IEEE Transactions on*
398 *Pattern Analysis and Machine Intelligence* **20**, 522-532 (1998).

399 47 Bille, P. J. T. c. s. A survey on tree edit distance and related problems. *Pattern Analysis and applications* **337**,
400 217-239 (2005).

401

Figures and Figure legends

a Evolutionary trajectories of variant B.1.1.7

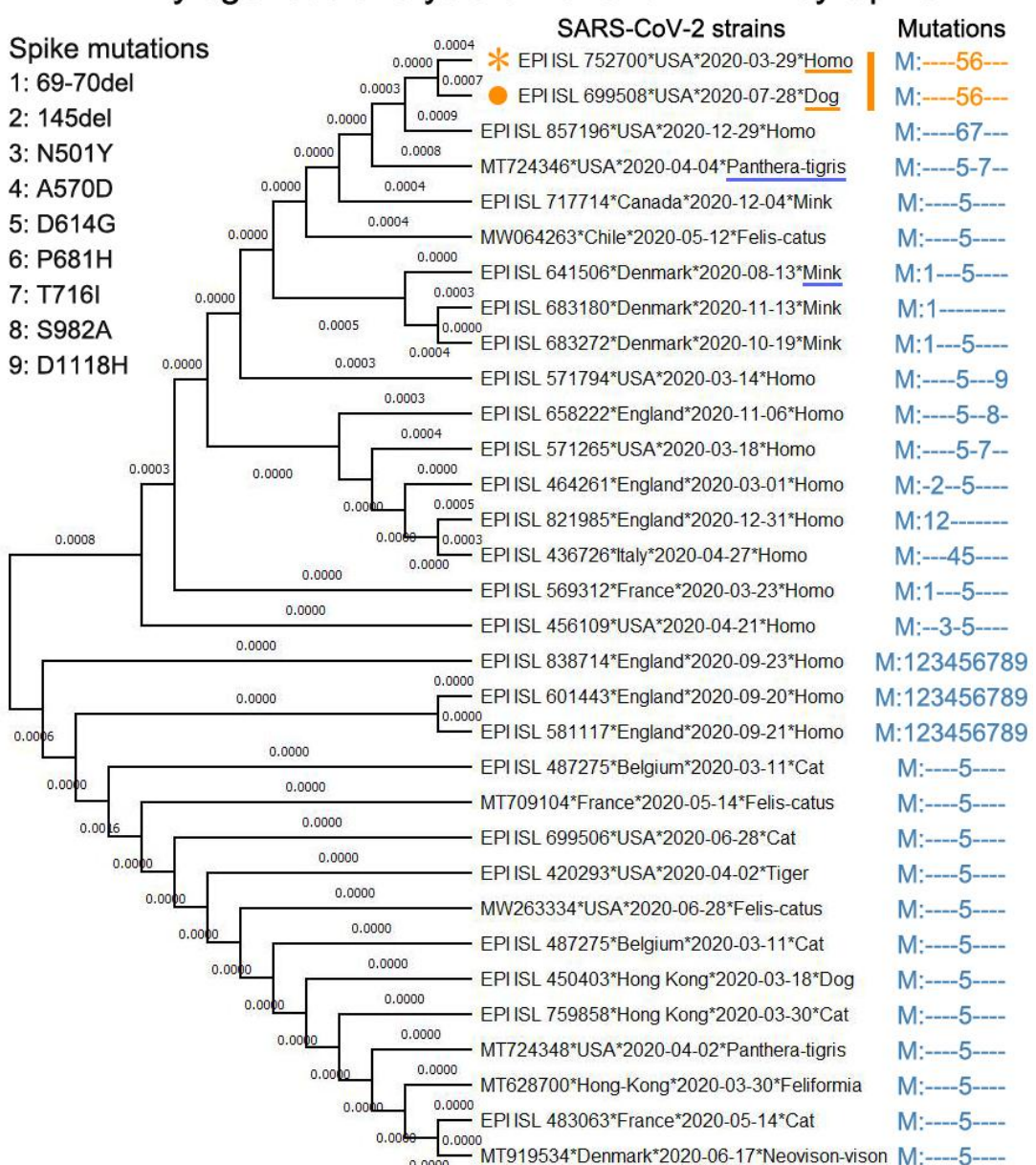


402

403 **Fig. 1 Evolutionary trajectories of variant B.1.1.7.** **a** Incremental mutations of variant B.1.1.7. The
404 digits in the upper-right-corner rectangle with dotted line indicate the labels of mutations. For
405 simplicity, the 69–70 deletions were labeled as “1”, and the other mutations “2”–“9” respectively. The
406 bottom nodes (rectangles) represent the variants with one mutation and the top one was the early
407 variant B.1.1.7. Each rectangle with solid line consists of lineage (e.g., B.1.243), number of strains
408 (e.g., N:2382), mutation sites (e.g., M:----56---), the earliest collection date (e.g., 20-03-29, i.e.,
409 2020-03-29), and collection location (e.g., USA). In the labels of the mutation sites, sign “-” indicated
410 the corresponding site did not mutate. All routes along the directions of the arrows are possible
411 evolutionary trajectories of lineage B.1.1.7, where the green one was the most probable mutation
412 trajectory. Large-scale SARS-CoV-2 analysis demonstrates that the early variant B.1.1.7 might not
413 have arisen spontaneously in the UK or within human hosts. **b** Coappearances of variant B.1.1.7
414 mutations. At least five mutations form a potential co-mutation pattern (coappearance rate > 95%). **c**
415 Possible transmission chains of variant B.1.1.7. Canidae, Mustelidae or Felidae, especially the
416 Canidae family (for example, dog) could be a possible host of the direct progenitor of variant B.1.1.7.

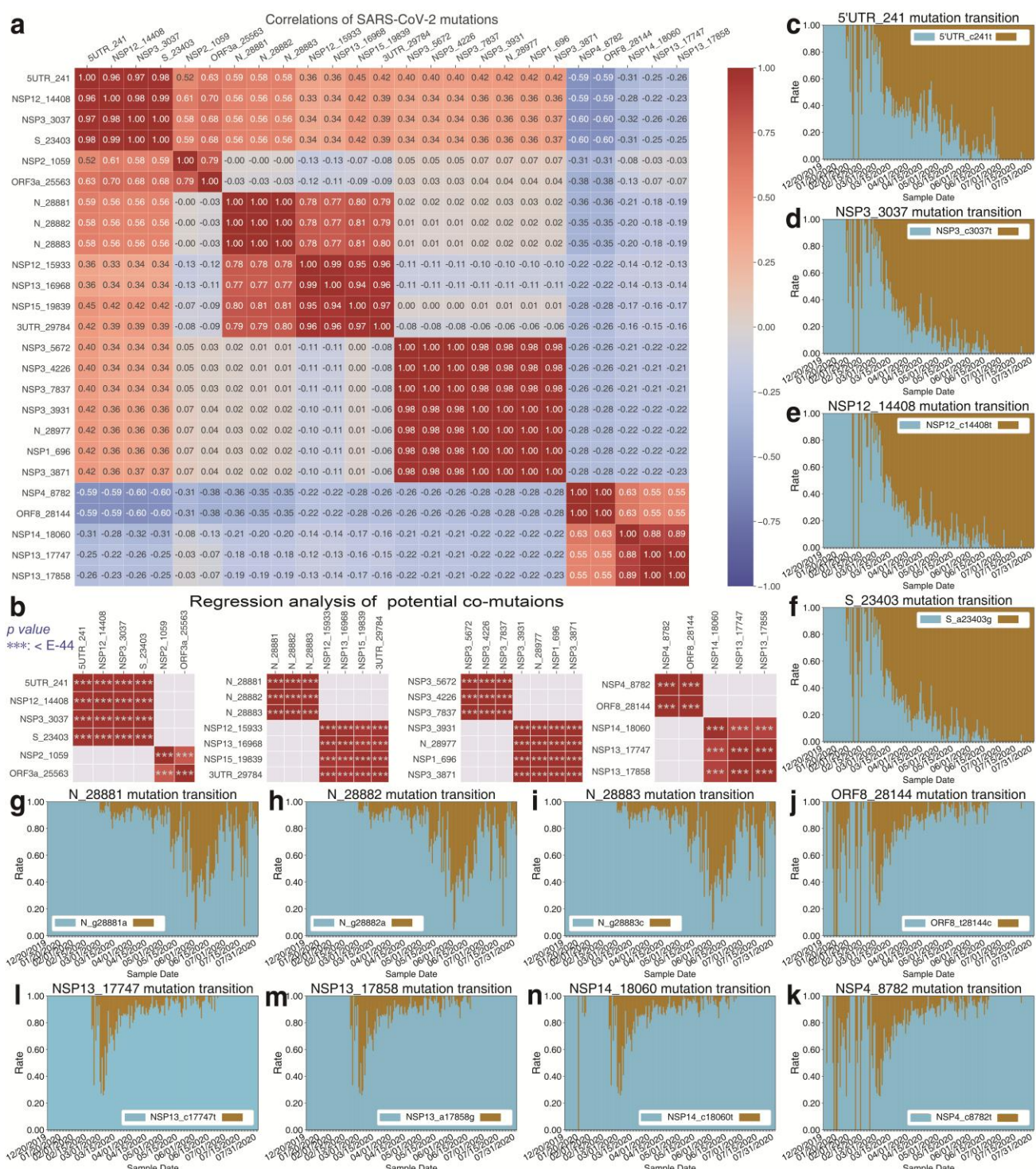
417

Phylogenetic analysis of variant B.1.1.7 by Spike

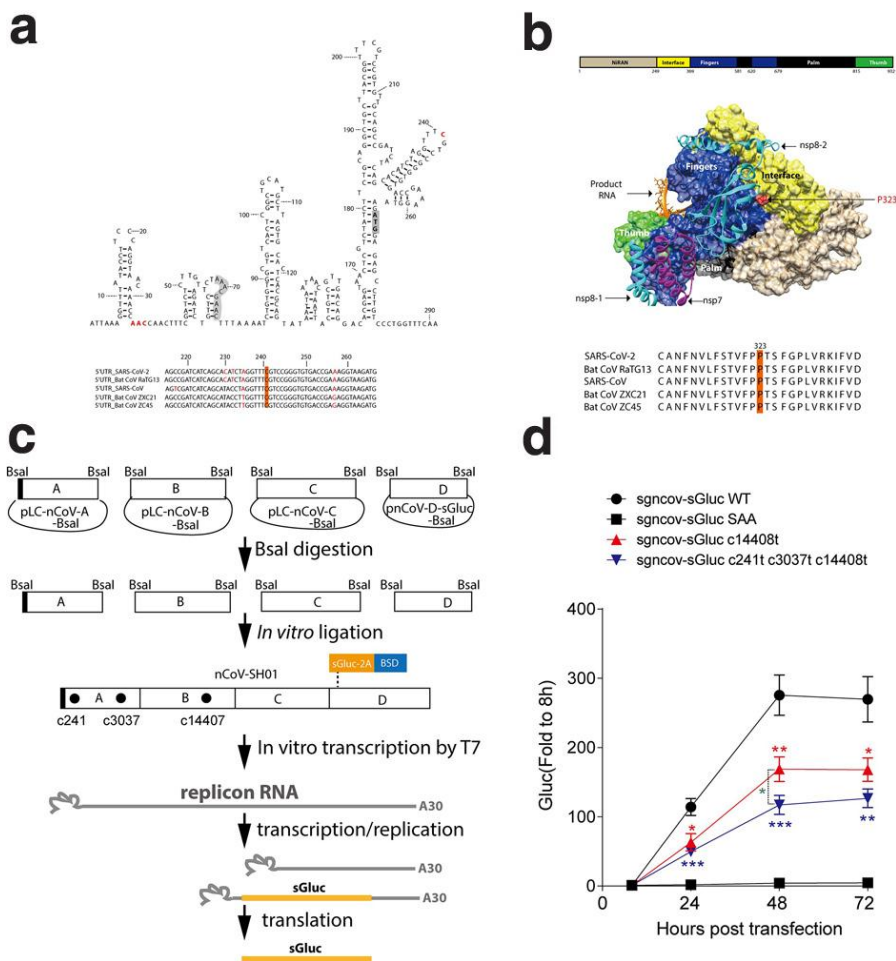


418

419 **Fig. 2 The Canidae family could be a possible host of the direct progenitor of variant B.1.1.7.**
420 The digits on the left of the figure indicate the labels of mutations, which correspond with the
421 mutation labels in [Fig. 1a](#). The strains shown in the center of the figure contain at least one spike
422 mutation of variant B.1.1.7. And these strain examples cover all existing SARS-CoV-2 viruses that
423 collected from animal hosts. The strain labeled by orange star corresponds with the star variant in [Fig.](#)
424 [1a](#). The strain with orange solid-round label was collected from a dog on 2020-07-28. Such two
425 strains share the same mutations “56” and have the minimum phylogenetic distance by MEGA tool.
426 Canidae, Mustelidae or Felidae, especially the Canidae family (for example, dog) could be a possible
427 host of the direct progenitor of variant B.1.1.7 based on existing stains collected before the end of
428 Jan. 2021.



430 **Fig. 3 The strong correlations suggest that the top 25 mutations form eight potential**
 431 **co-mutation patterns. a** The correlation heatmap of the top 25 mutations. These mutations could be
 432 grouped into several clusters with high Pearson-correlation-coefficient (PCC). **b** Regression analysis
 433 of mutations shows that eight clusters all denote the statistical significance level: ***p value < E-44. **c**
 434 to **k** show the transitions of the high-frequency mutations. The sky-blue represents the rate per day of
 435 initial residue in population and the golden the rate per day of substitution/mutant. These mutation
 436 transitions provide further evidence that the above mutations potentially form co-mutation patterns.



437

438 **Fig. 4 Dominant co-mutation attenuates viral replication.** **a** Predicted RNA structure of the
439 SARS-CoV-2 5'UTR. RNA structure of the 400-nt 5'UTR was predicted by “RNAstructure”
440 (<http://rna.urmc.rochester.edu/RNAstructureWeb>). The start codon for nsp1 is grey, the TRS-L is
441 orange, and the mutated nucleotides are red. The bottom panel shows the alignment of the 5'UTR of
442 SARS-CoV-2 with 5'UTRs of related viruses, with c241 highlighted. **b** Structure of SARS-CoV-2
443 RdRp/RNA complex. The structure of SARS-CoV-2 RdRp/RNA complex (PDB, 6X2G) was visualized
444 by Chimera (UCSF). The P323 mutation is highlighted in red, with the alignment of the amino acid
445 sequences of SARS-CoV-2 and related viruses near the P323 position. **c** Schematic of the *in-vitro*
446 ligation system for SARS-CoV-2 replicon. Four plasmids encompassing the viral genome were
447 digested by Bsal to release the four fragments. After gel purification, the fragments were ligated by
448 T4 ligase. The ligation products were purified and used as template for RNA *in-vitro* transcription.
449 sGluc, secreted *Gaussia* luciferase; 2A, foot-and-mouth disease virus (FMDV) 2A peptide; BSD,
450 blasticidin. **d** Huh7 cells were co-transfected with *in-vitro* transcribed replicon RNA (WT or the
451 indicated mutants) and an mRNA encoding the SARS-CoV-2 N protein. The luciferase activity in the
452 supernatants was measured at the time points indicated. Medium was changed at 8 hours
453 post-transfection. Data are shown as mean±SEM (n=8). SAA, the NSP12 polymerase active-site
454 mutant. Unpaired Student's t-test was performed between the mutants and wild type (WT) and
455 between the mutants as indicated (statistical significance level: *p value<0.05, **p value<0.01, ***p
456 value<0.001).